Supporting informantion for

Luminescent porous metal–organic gels for efficient adsorption and sensitive detection of chlortetracycline hydrochloride assisted by smartphones and test paper-based analytical device

Meijun Liu [a,1], Shuai Xia [a,1], Zhi Liu [b], Taigang Ma [a], Zhisheng Liu [b], Yangxue Li [a, c, *], Donglei Zou [a, *]

[a] *Key Lab of Groundwater Resources and Environment (Ministry of Education), Jilin Provincial Key Laboratory of Water Resources and Environment, Jilin University, 2519 Jiefang Road, Changchun 130021, P. R. China*

[b] *School of Municipal and Environmental Engineering, Jilin Jianzhu University, 5088 Xincheng Street, Changchun 130118, P. R. China*

[c] *Chongqing Research Institute, Jilin University, Chongqing 401123, P. R. China*

Supporting Information contains:

Experimental Section:

Figures:

Experimental Section:

The equations for calculating the quenching effect and LOD：

$$I_0 / I = 1 + K_{SV} \times [C] \quad (1)$$

$$LOD = 3\sigma / K_{SV} \quad (2)$$

Where I_0 and I are on behalf of the fluorescent intensities of JLUE-MOG-9 in the absence and existence of CTC with various concentrations, respectively; K_{SV} denotes the Stern–Volmer quenching constant; C is the CTC concentration in solution; LOD represents the detection limit, and σ is the standard derivation of the blank sample (10 times).

The equation for calculating the CTC concentration from R, G and B values：

$$CR = \frac{(\frac{R_s}{R_r} + \frac{G_s}{G_r} + \frac{B_s}{B_r})}{3} \quad (3)$$

Where the R_s, G_s and B_s represented the R, G and B values of samples; R_r, G_r and B_r were on behalf of the R, G and B values of blank solution.

The summary of utilized models in manuscript：

Adsorption kinetic models	Equations
Pseudo-first kinetic model	$\ln(q_e - q_t) = \ln q_e - k_1 t$
Pseudo-second kinetic model	$\frac{t}{q_t} = \frac{1}{k_2 q_e^2} + \frac{t}{q_e}$
Intra-particle diffusion model	$q_t = k_i t^{1/2} + C$

Where q_e and q_t are on behalf of the adsorbed amounts of CTC at equilibrium stage and time t ($mg \cdot g^{-1}$), respectively; k_1, k_2 and k_i denote the pseudo-first-order kinetic model rate constant (h^{-1}), the pseudo-second-order kinetic model rate constant ($g \cdot mg^{-1} \cdot h^{-1}$) and the intra-particle diffusion model rate constant ($mg \cdot g^{-1} \cdot h^{-1/2}$), respectively; C is the intercept ($mg \cdot g^{-1}$).

Adsorption Isotherm models	Equations
Freundlich	$\ln q_e = \ln K_F + \frac{1}{n} \ln C_e$
Langmuir	$\frac{C_e}{q_e} = \frac{1}{K_L} + \frac{a_L C_e}{K_L}$
Temkin	$q_e = B \ln K_T + B \ln C_e$

Where q_e represents the same meaning as above; C_e is the equilibrium concentration of CTC in solution (mg·L^{-1}); K_L and a_L are the Langmuir isotherm constants; K_F is the Freundlich isotherm constant; K_T is the Temkin constant (L·mg^{-1}); B is related to the heat of adsorption (J·mol^{-1}); $1/n$ is a heterogeneity factor.

Figures

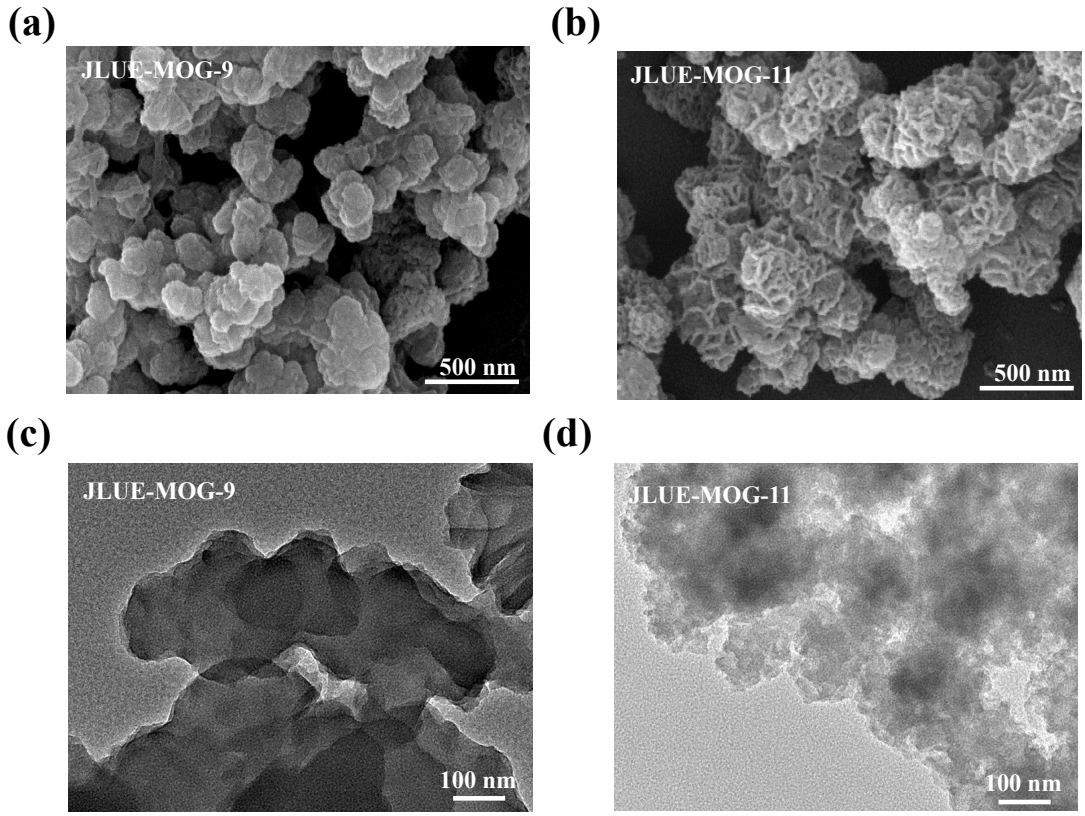

Fig. S1. The SEM results of (a) JLUE-MOG-9 and (b) JLUE-MOG-11. The TEM results of (c) JLUE-MOG-9 and (d) JLUE-MOG-11.

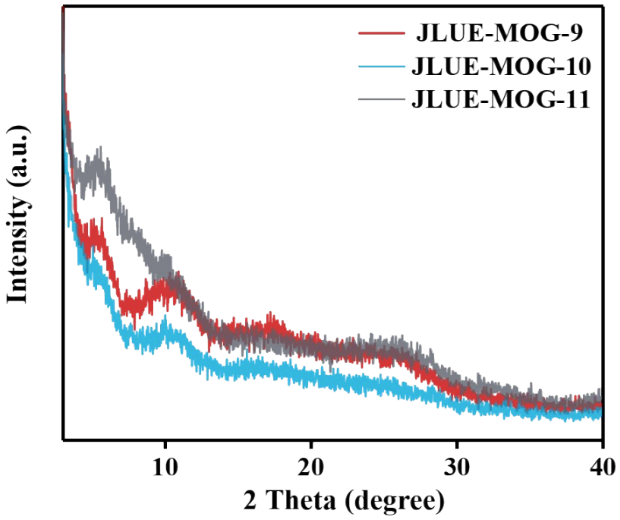

Fig. S2. The XRD patterns of the JLUE-MOGs.

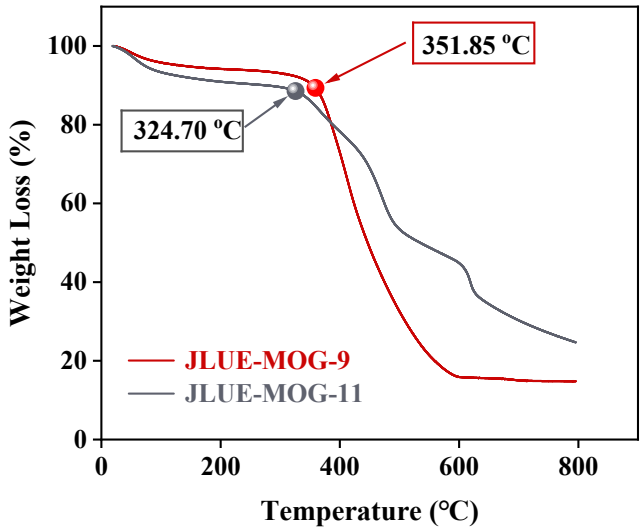

Fig. S3. The TGA curves of JLUE-MOG-9 and JLUE-MOG-11.

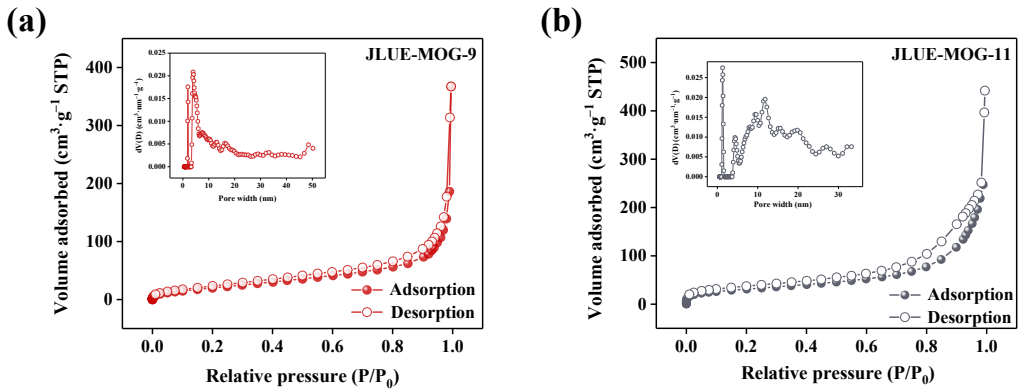

Fig. S4. The BET results of (a) JLUE-MOG-9 and (b) JLUE-MOG-11, insert: the pore size distributions of (a) JLUE-MOG-9 and (b) JLUE-MOG-11.

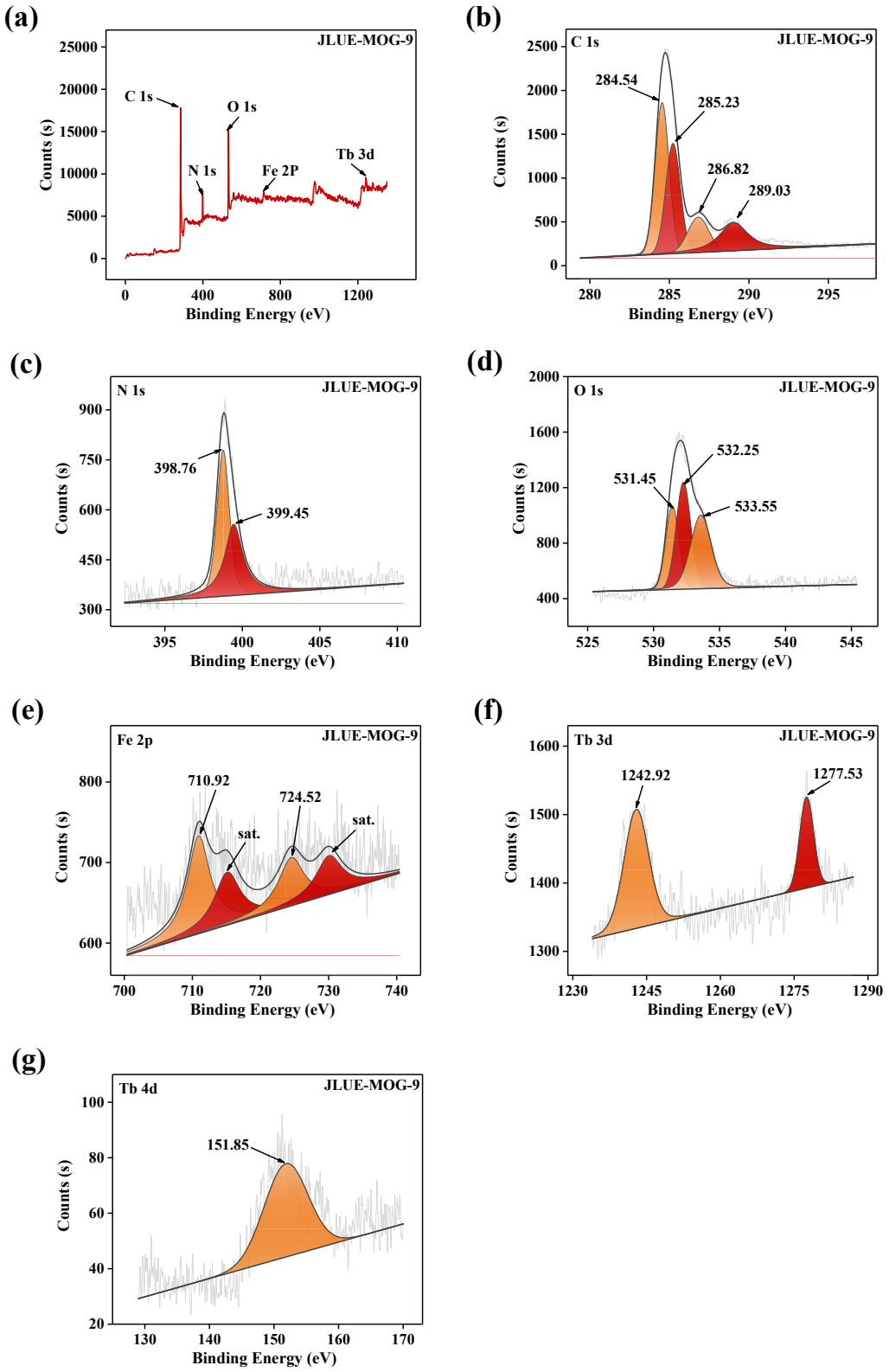

Fig. S5. The XPS spectra of JLUE-MOG-9: (a) Survey spectrum. (b) High-solution spectrum of C 1s. (c) High-solution spectrum of N 1s. (d) High-solution spectrum of O 1s. (e) High-solution spectrum of Fe 2p. (f) High-solution spectrum of Tb 3d. (g) High-solution spectrum of Tb 4d.

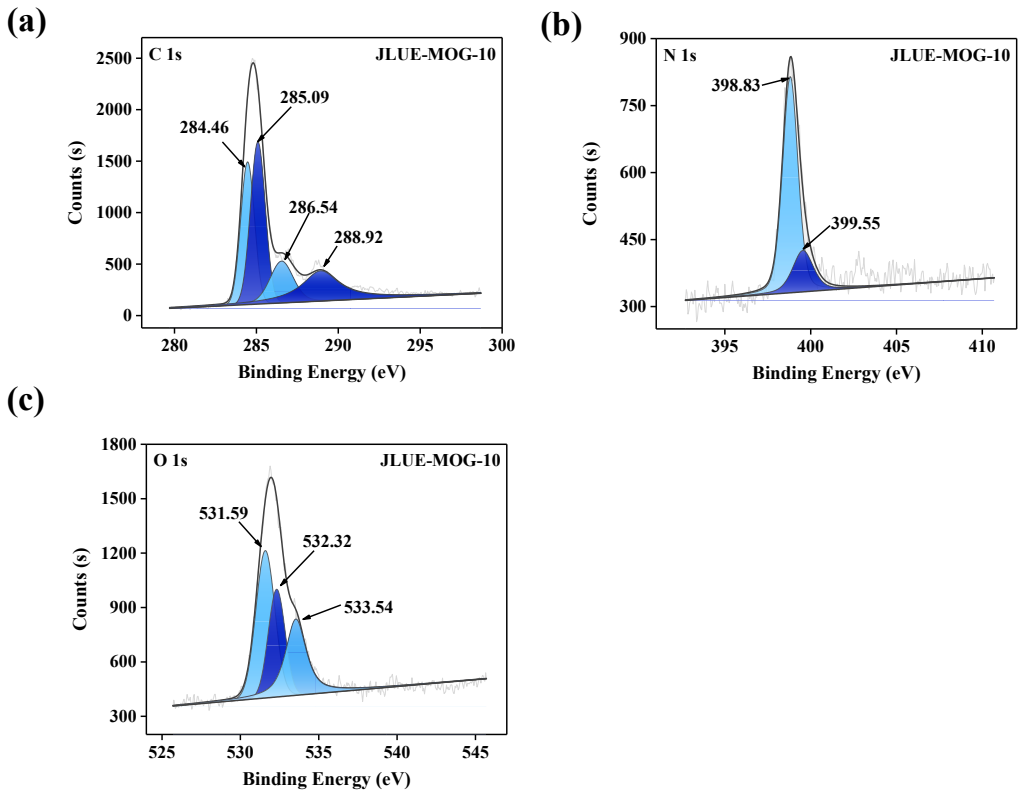

Fig. S6. The XPS spectra of JLUE-MOG-10: (a) High-solution spectrum of C 1s. (b) High-solution spectrum of N 1s. (c) High-solution spectrum of O 1s.

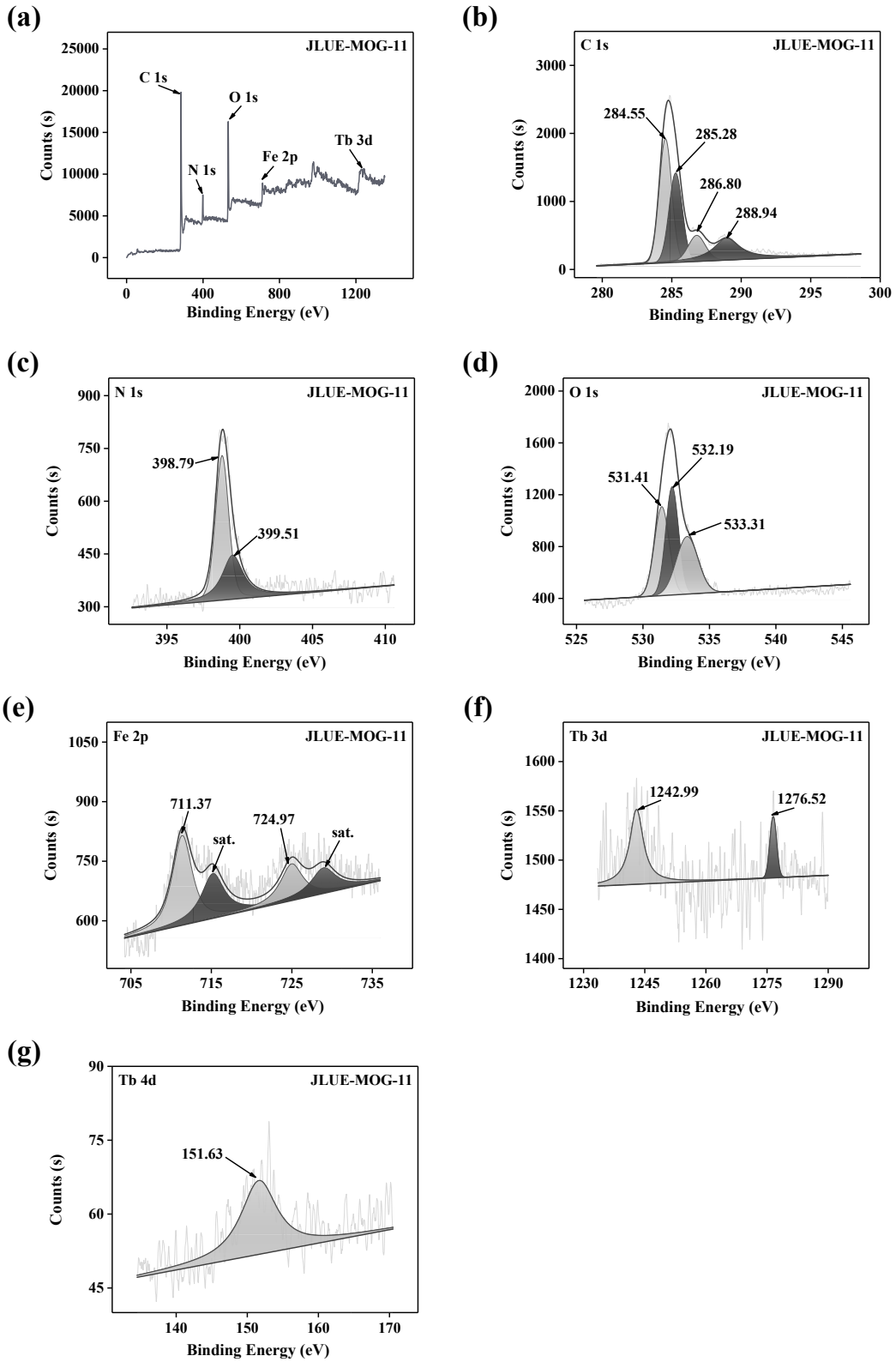

Fig. S7. The XPS spectra of JLUE-MOG-11: (a) Survey spectrum. (b) High-solution spectrum of C 1s. (c) High-solution spectrum of N 1s. (d) High-solution spectrum of O 1s. (e) High-solution spectrum of Fe 2p. (f) High-solution spectrum of Tb 3d. (g) High-solution spectrum of Tb 4d.

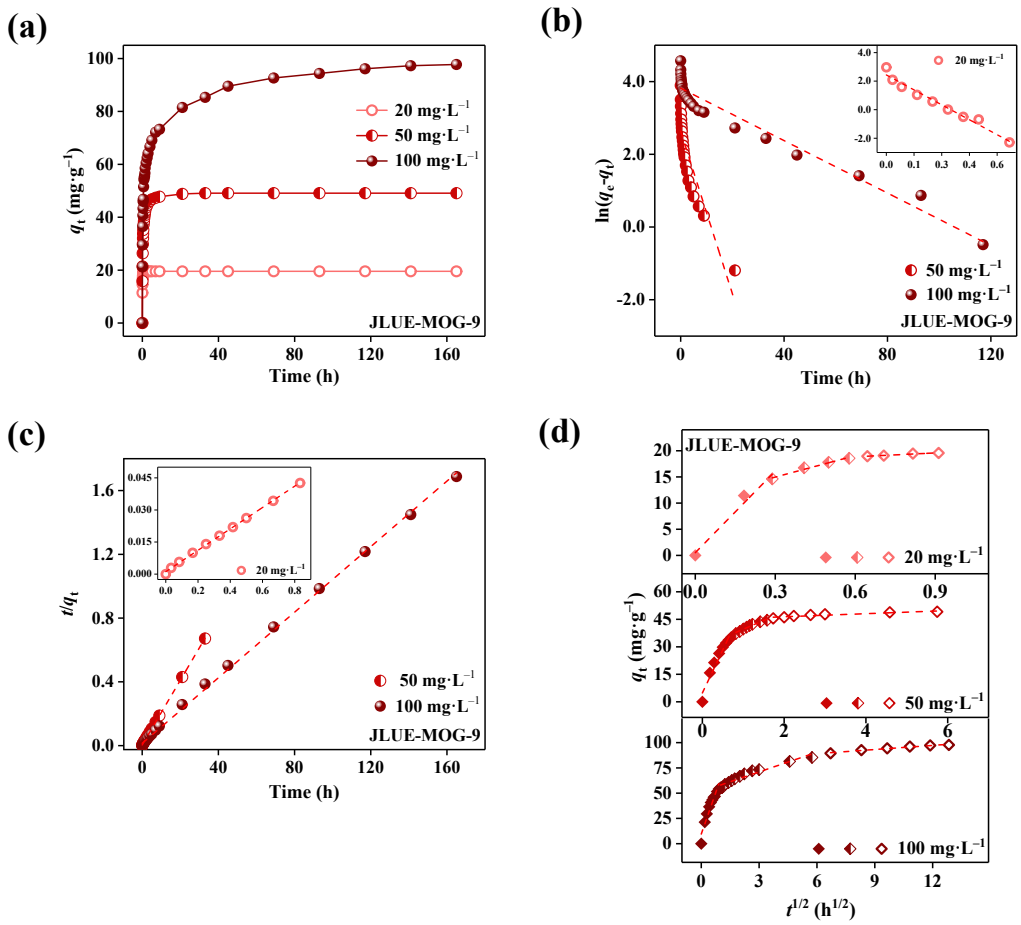

Fig. S8. (a) Adsorptive removal and (b) corresponding pseudo-first-order kinetic model, (c) pseudo-second-order kinetic model and (d) intra-particle diffusion model fittings for the CTC adsorption by JLUE-MOG-9.

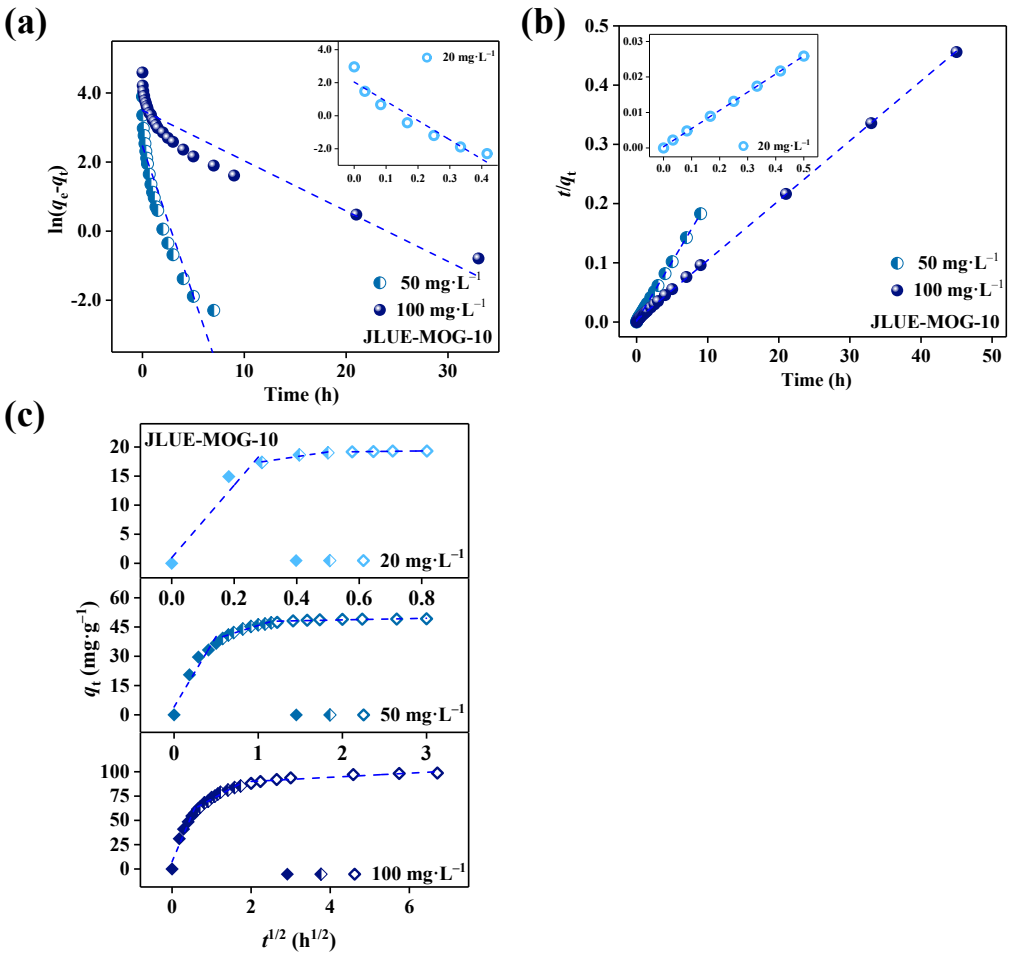

Fig. S9. (a) Pseudo-first-order kinetic model, (b)pseudo-second-order kinetic model and (c) intra-particle diffusion model fittings for the CTC adsorption by JLUE-MOG-10.

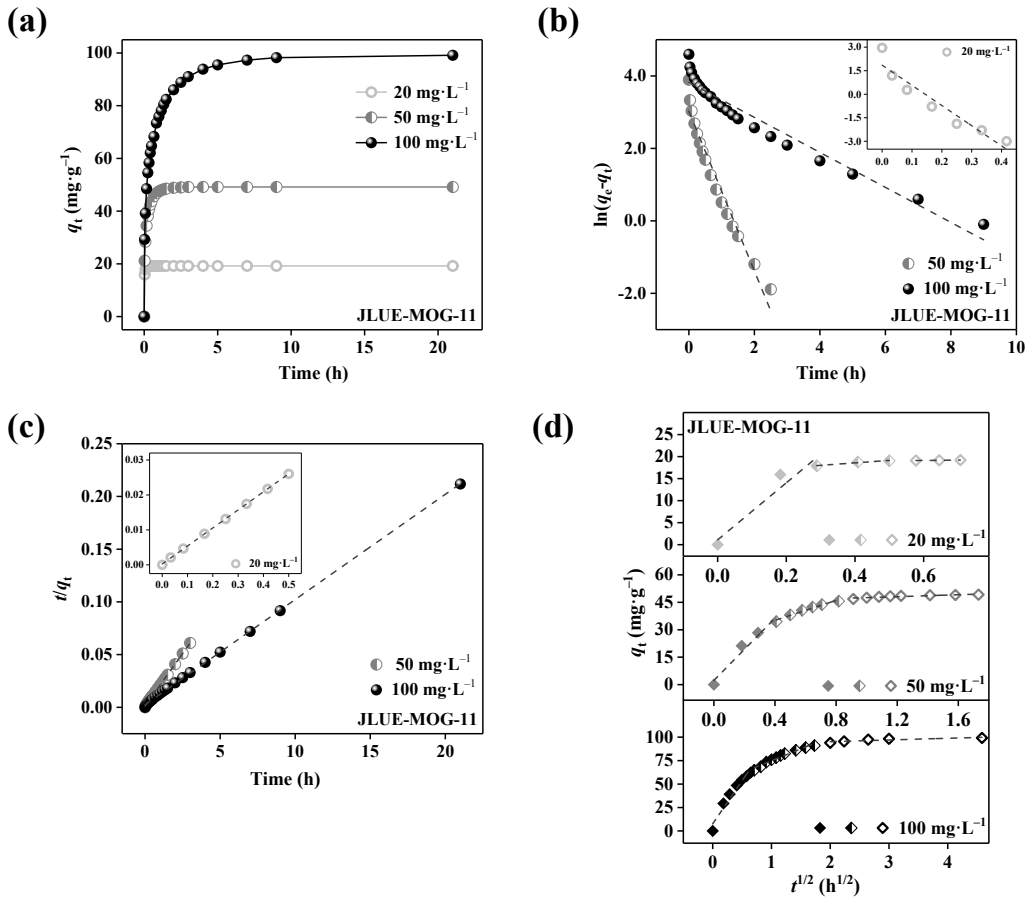

Fig. S10. (a) Adsorptive removal and (b) corresponding pseudo-first-order kinetic model, (c) pseudo-second-order kinetic model and (d) intra-particle diffusion model fittings for the CTC adsorption by JLUE-MOG-11.

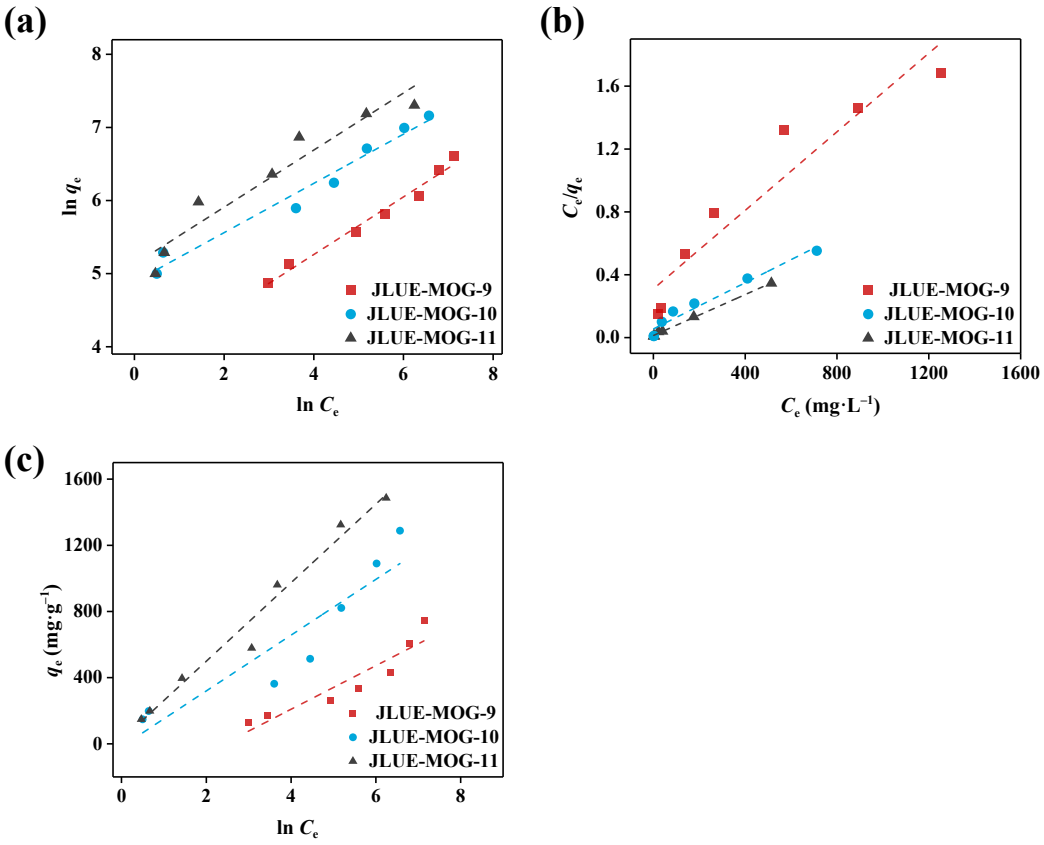

Fig. S11. (a) The Langmuir , (b) Freundlich and (c) Temkin linear fittings for CTC adsorptive removal by the JLUE-MOGs at 25 °C.

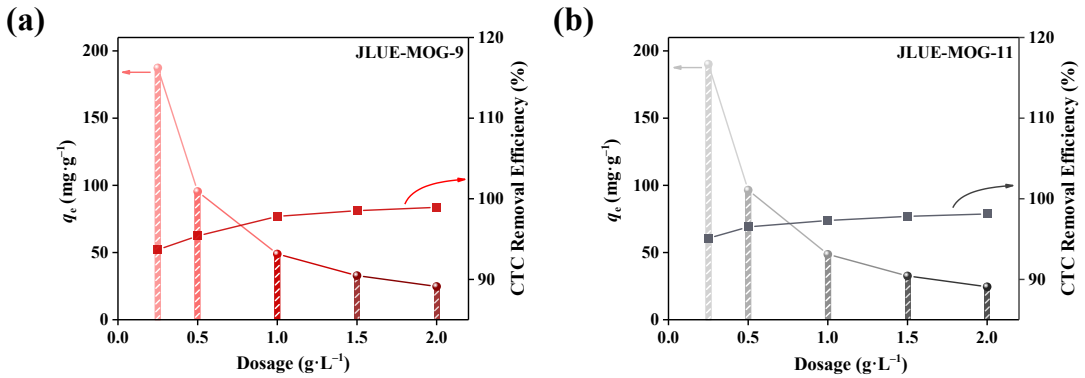

Fig. S12. Variance in CTC removal efficiencies and adsorption capacities per unit weight adsorbents (q_e) of (a) JLUE-MOG-9 and (b) JLUE-MOG-11 as a function of adsorbent dosage.

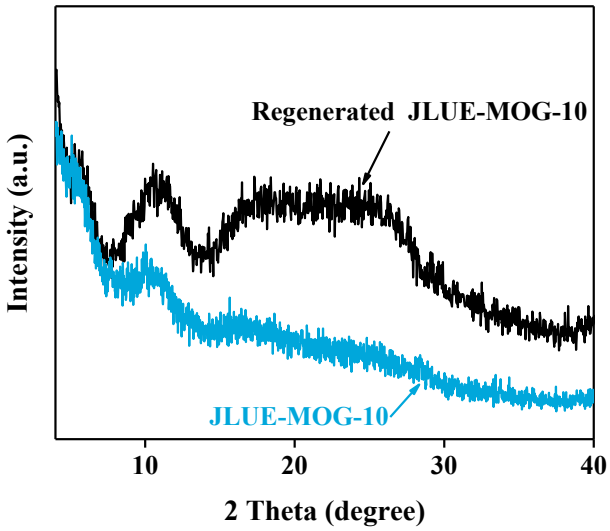

Fig. S13. The XRD spectra of JLUE-MOG-10 and regenerated JLUE-MOG-10.

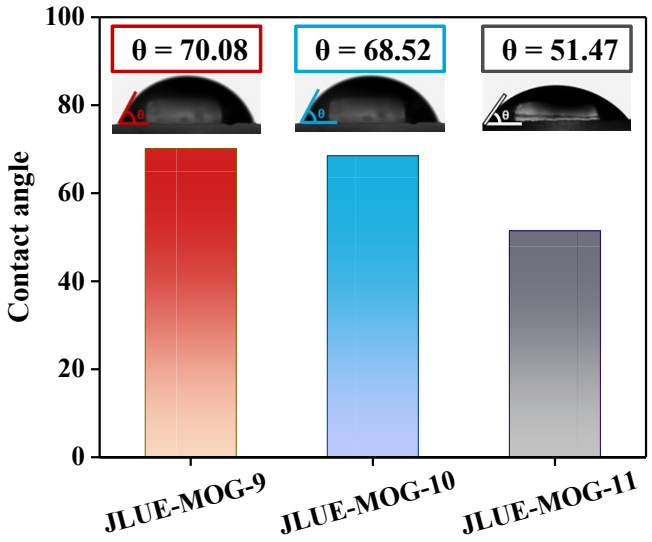

Fig. S14. The contact angles of JLUE-MOGs in distilled water.

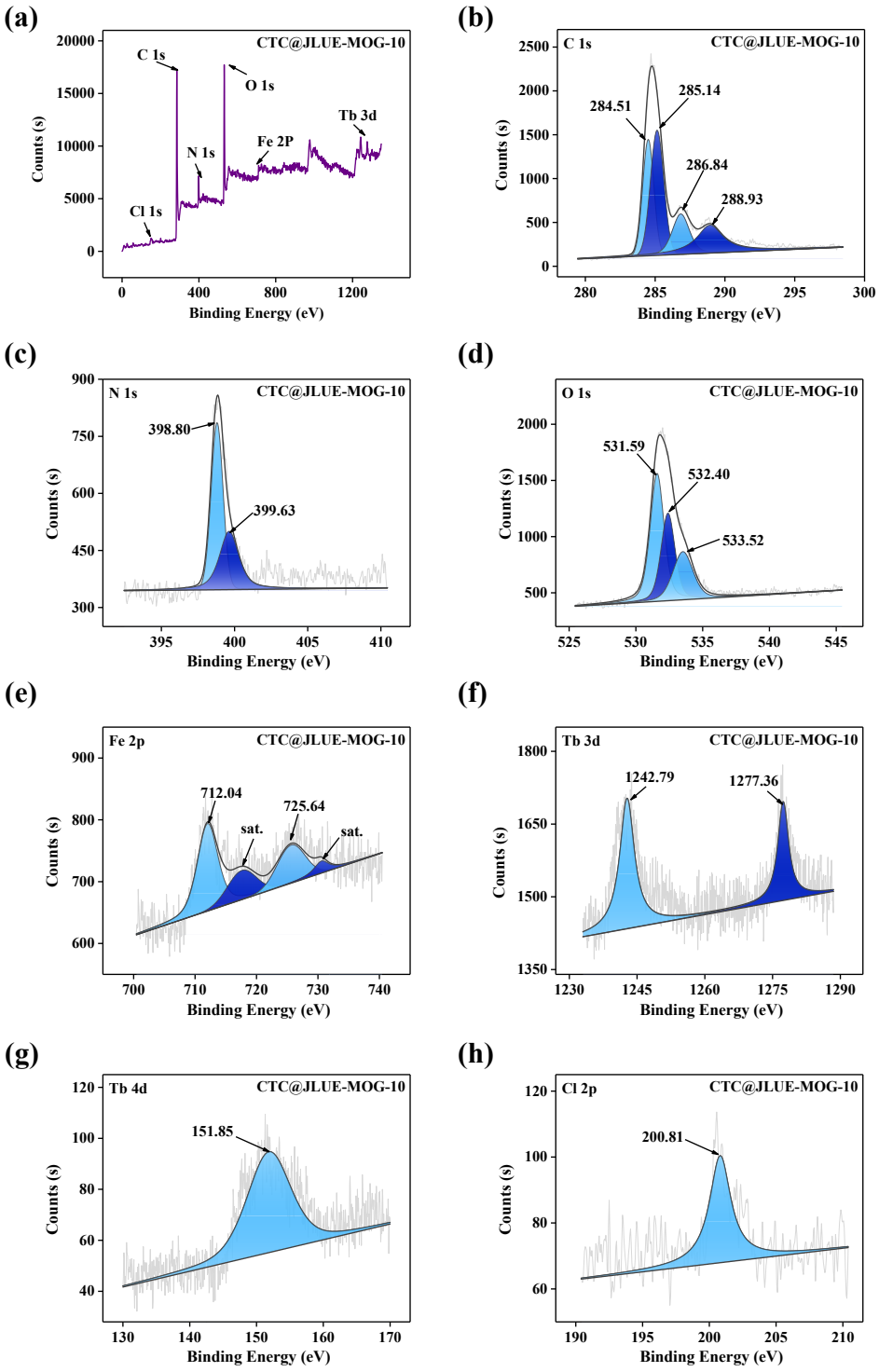

Fig. S15. The XPS spectra of CTC@JLUE-MOG-10: (a) Survey spectrum. (b) High-solution spectrum of C 1s. (c) High-solution spectrum of N 1s. (d) High-solution spectrum of O 1s. (e) High-solution spectrum of Fe 2p. (f) High-solution spectrum of Tb 3d. g) High-solution spectrum of Tb 4d. (h) High-solution spectrum of Cl 2p.

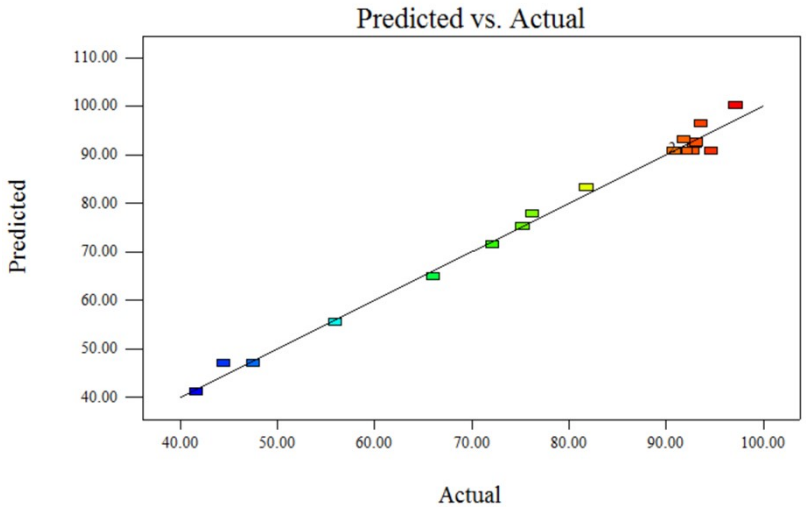

Fig. S16. The actual results plotted against the predicted responses derived from the FCCD model of CTC removal.

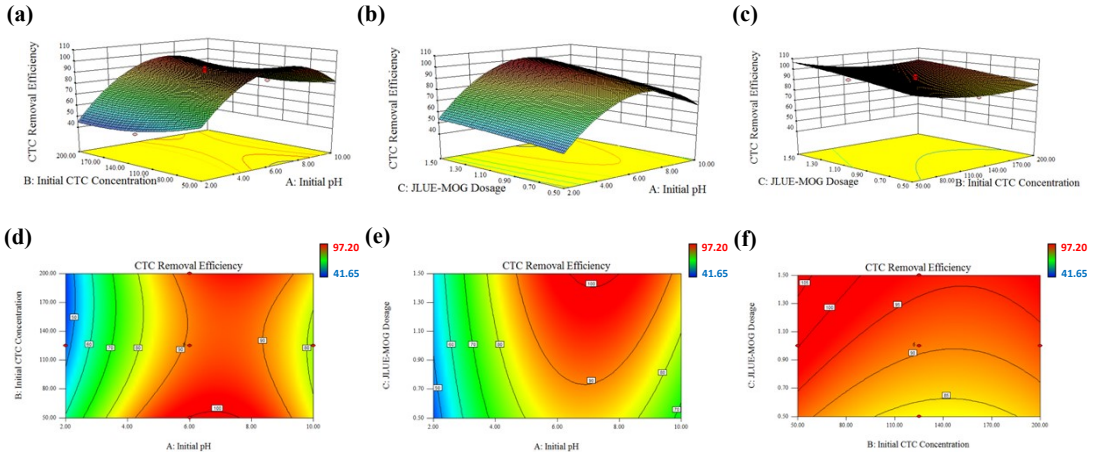

Fig. S17. 3D surface plots and corresponding contour plots for interactions between initial pH and initial CTC concentration (a, d), initial pH and JLUE-MOG dosage (b, e) and initial CTC concentration and JLUE-MOG dosage (c, f).

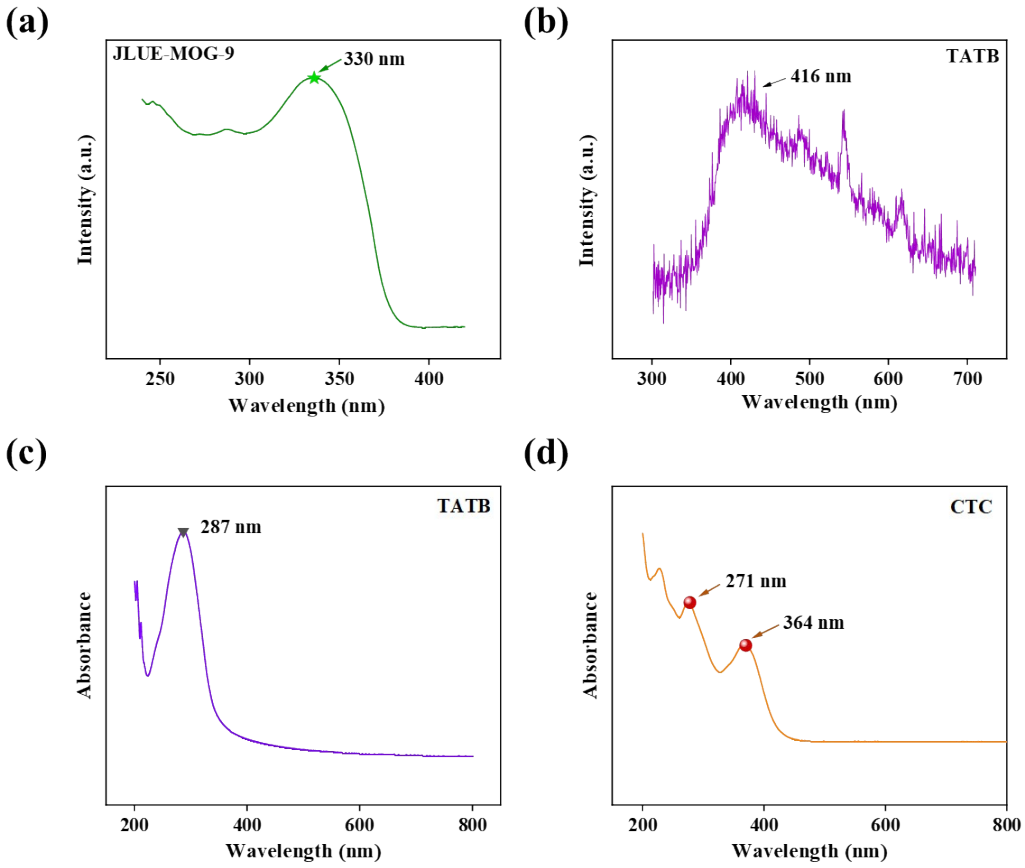

Fig. S18. (a) The excitation spectrum of JLUE-MOG-9. (b) The emission spectrum of TATB. (c) The UV-Vis absorption spectrum of TATB. (d) The UV-Vis absorption spectrum of CTC.

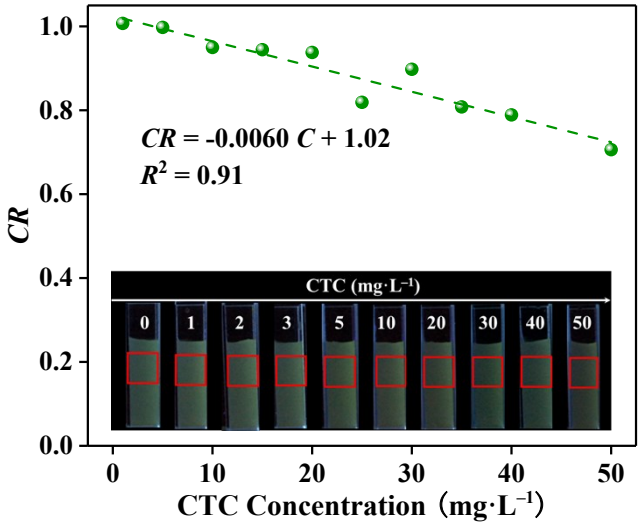

Fig. S19. The plot between *CR* values and various CTC concentrations, insert: the digital photos of fluorescence of JLUE-MOG-9 under 254 nm UV light.

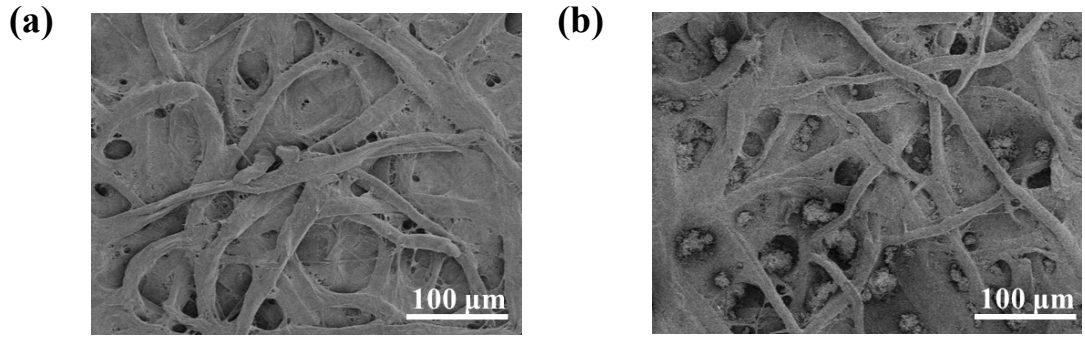

Fig. S20. The SEM results of (a) blank paper and (b) JLUE-MOG-9@paper.

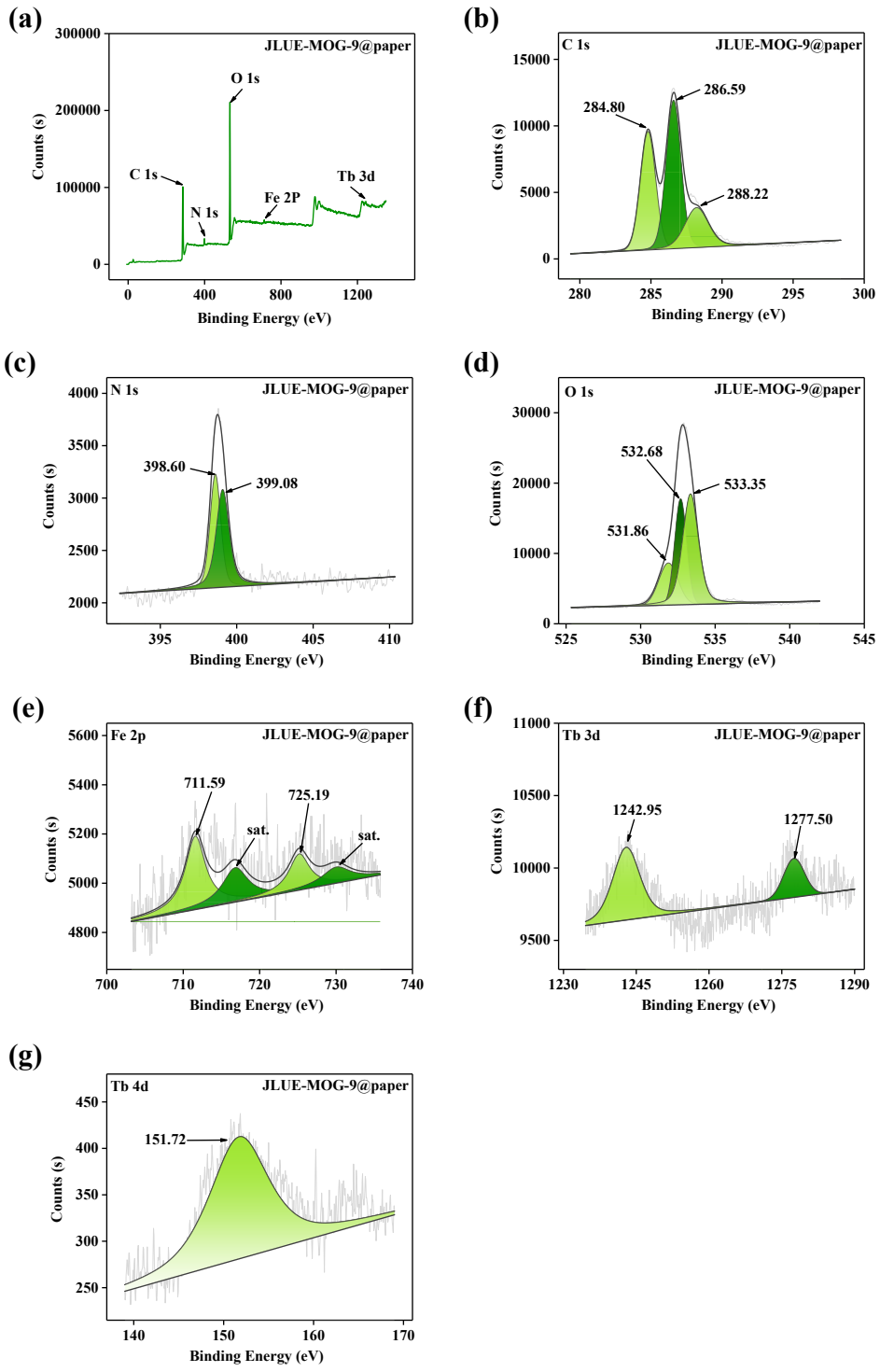

Fig. S21. The XPS spectra of JLUE-MOG-9@paper: (a) The survey spectrum. (b) High-solution spectrum of C 1s. (c) High-solution spectrum of N 1s. (d) High-solution spectrum of O 1s. (e) High-solution spectrum of Fe 2p. (f) High-solution spectrum of Tb 3d. (g) High-solution spectrum of Tb 4d.

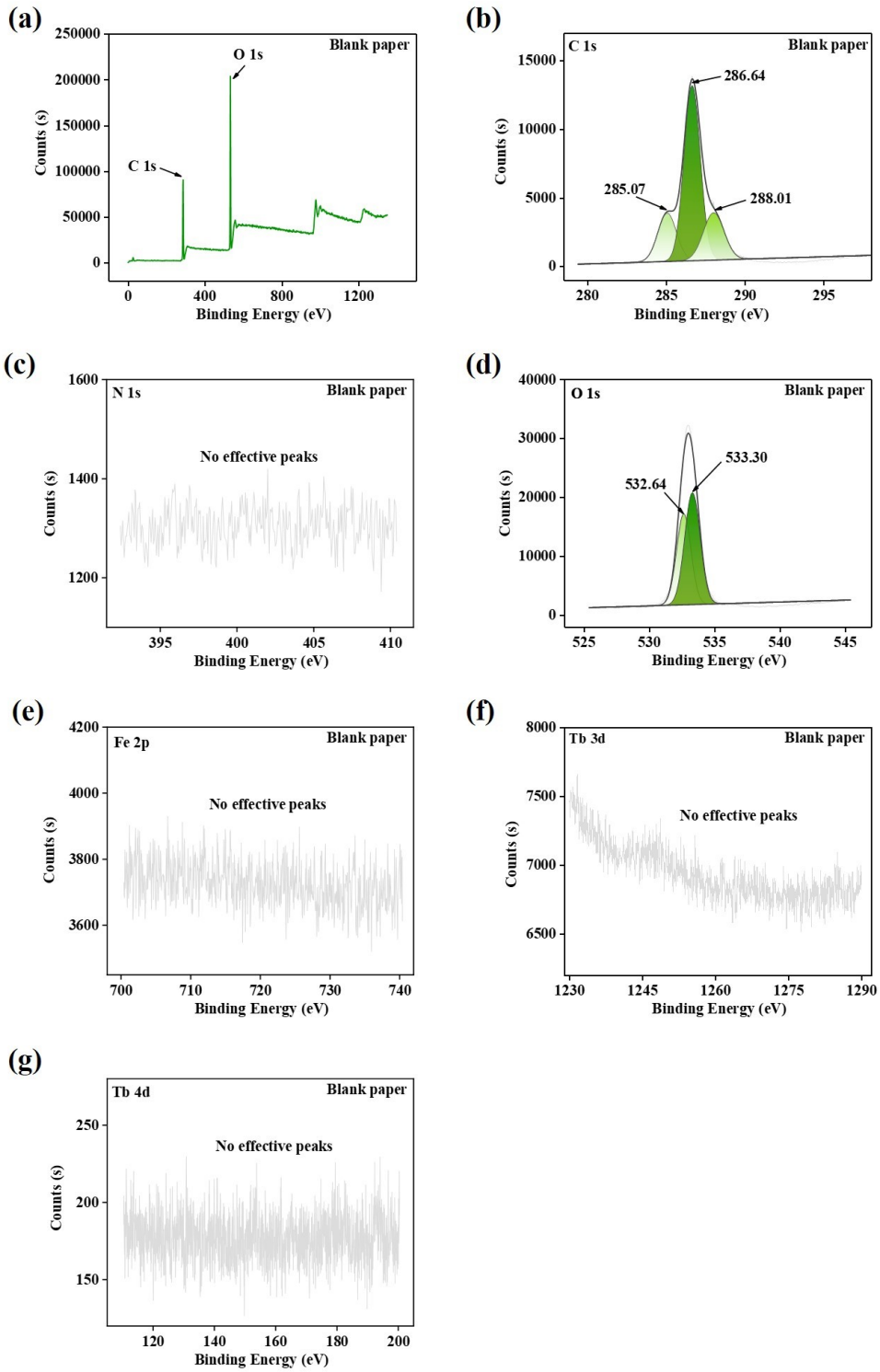

Fig. S22. The XPS spectra of blank paper: (a) The survey spectrum. (b) High-solution spectrum of C 1s. (c) High-solution spectrum of N 1s. (d) High-solution spectrum of O 1s. (e) High-solution spectrum of Fe 2p. (f) High-solution spectrum of Tb 3d. (g) High-solution spectrum of Tb 4d.

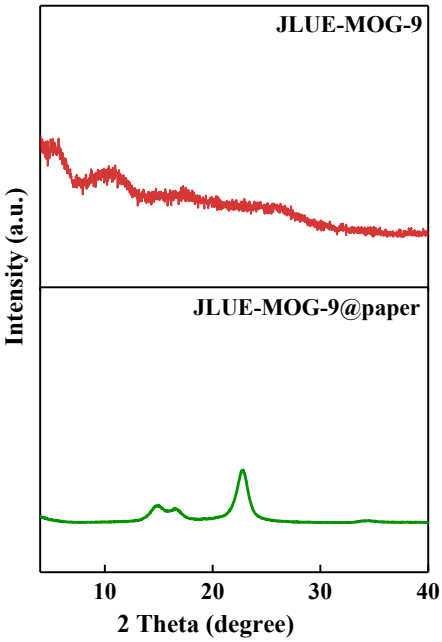

Fig. S23. The XRD spectra of JLUE-MOG-9 and JLUE-MOG-9@paper.

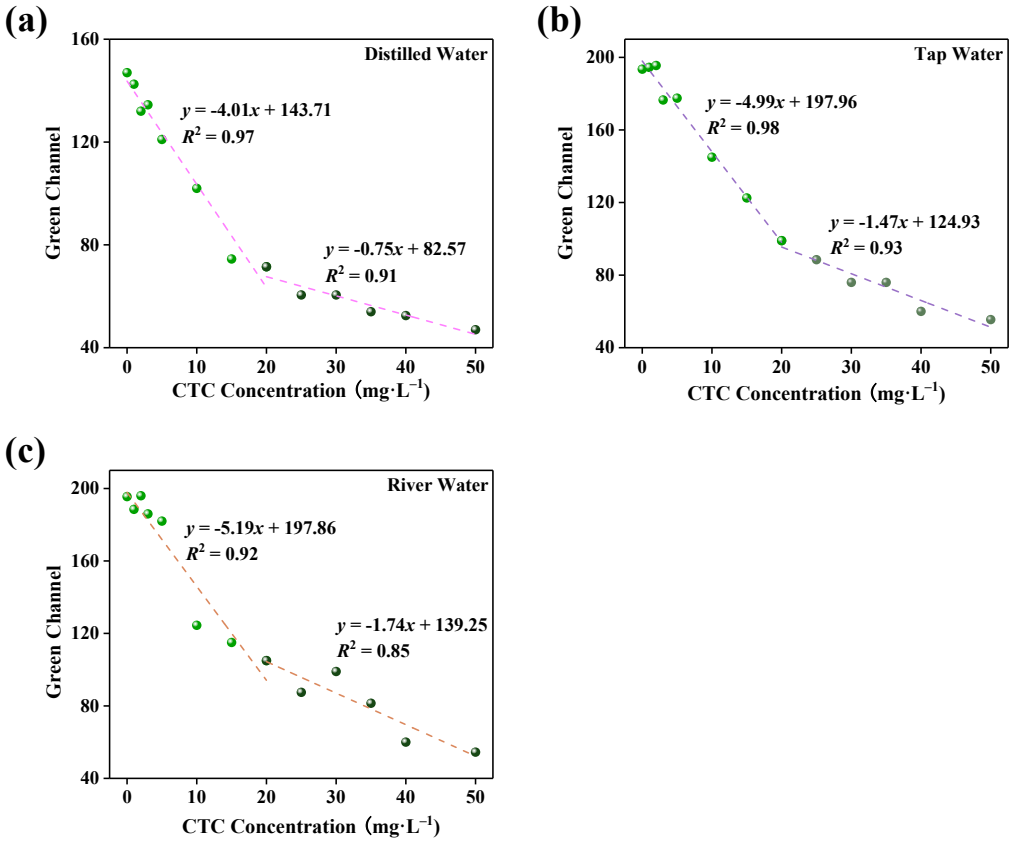

Fig. S24. The relationships between the values of green channel of JLUE-MOG-9@paper and various CTC concentrations in (a) distilled water, (b) tap water and (c) river water.

Tables

Table S1. Pseudo-first-order kinetic model parameters for CTC adsorption by JLUE-MOG-9, JLUE-MOG-10 and JLUE-MOG-11.

JLUE-MOGs	C_0 (mg·L^{-1})	$q_{e,exp}$ (mg·g^{-1})	Removal Efficiency（%）	Pseudo-first-order kinetics			
				k_1 (h^{-1})	$q_{e1,theor}$ (mg·g^{-1})	Δq_1（%）	R^2
JLUE-MOG-9	20	19.57	97.32	6.98	11.42	71.39	0.97
	50	49.11	98.22	0.22	14.00	250.68	0.78
	100	97.75	97.75	0.04	45.54	114.63	0.94
JLUE-MOG-10	20	19.31	96.82	11.66	7.70	150.74	0.92
	50	49.21	98.42	0.87	11.79	317.46	0.86
	100	98.91	98.71	0.15	32.96	200.12	0.86
JLUE-MOG-11	20	19.21	95.30	12.86	6.38	201.26	0.91
	50	49.16	98.32	2.20	20.66	137.90	0.95
	100	99.11	99.11	0.48	45.65	117.12	0.94

Table S2. Pseudo-second-order kinetic model parameters for CTC adsorption by JLUE-MOG-9, JLUE-MOG-10 and JLUE-MOG-11.

JLUE-MOGs	C_0 (mg·L^{-1})	$q_{e,exp}$ (mg·g^{-1})	Removal Efficiency (%)	Pseudo-second-order kinetics			
				k_2 (g·mg^{-1}·h^{-1})	$q_{e2,theor}$ (mg·g^{-1})	Δq_2 (%)	R^2
JLUE-MOG-9	20	19.57	97.32	2.45	20.02	2.27	0.99
	50	49.11	98.22	0.10	49.31	0.40	0.99
	100	97.75	97.75	0.01	97.28	0.49	0.99
JLUE-MOG-10	20	19.31	96.82	7.45	19.54	1.15	0.99
	50	49.21	98.42	0.29	49.63	0.84	0.99
	100	98.91	98.71	0.03	99.11	0.20	0.99
JLUE-MOG-11	20	19.21	95.30	11.25	19.37	0.82	0.99
	50	49.16	98.32	0.34	50.18	2.02	0.99
	100	99.11	99.11	0.04	100.20	1.09	0.99

Table S3. Intra-particle diffusion model parameters for CTC adsorption by JLUE-MOG-9, JLUE-MOG-10 and JLUE-MOG-11.

Parameters	Intra-particle diffusion model								
	JLUE-MOG-9			JLUE-MOG-10			JLUE-MOG-11		
C_0 ($mg \cdot L^{-1}$)	20	50	100	20	50	100	20	50	100
$k_{i,1}$ ($mg \cdot g^{-1} \cdot h^{-1/2}$)	51.94	47.04	54.62	62.44	72.43	96.03	64.76	85.08	91.75
C_1 ($mg \cdot g^{-1}$)	0.52	4.84	9.48	0.95	4.00	7.48	1.10	2.29	7.63
R^2	0.97	0.94	0.92	0.94	0.93	0.93	0.93	0.96	0.95
$k_{i,2}$ ($mg \cdot g^{-1} \cdot h^{-1/2}$)	13.64	9.64	6.50	8.04	13.59	22.19	5.58	27.25	25.37
C_2 ($mg \cdot g^{-1}$)	10.88	29.95	51.55	15.13	32.23	49.55	16.35	24.23	49.44
R^2	0.99	0.96	0.94	0.94	0.95	0.95	0.96	0.97	0.96
$k_{i,3}$ ($mg \cdot g^{-1} \cdot h^{-1/2}$)	2.45	0.84	1.36	0.67	0.85	2.13	0.78	2.59	1.79
C_3 ($mg \cdot g^{-1}$)	17.37	44.72	81.02	18.79	46.95	85.79	18.66	44.98	91.62
R^2	0.95	0.89	0.97	0.81	0.73	0.89	0.99	0.84	0.74

Table S4. Freundlich, Langmuir and Temkin adsorption isotherm model parameters for CTC adsorption by JLUE-MOG-9, JLUE-MOG-10 and JLUE-MOG-11 at 25 °C.

JLUE-MOGs	Freundlich isotherm			Langmuir isotherm			Temkin isotherm		
	n	K_F	R^2	q_m (mg·g^{-1})	K_L	R^2	K_T (L·mg^{-1})	B (J·mol^{-1})	R^2
JLUE-MOG-9	2.54	39.81	0.98	912.47	3.23	0.91	0.089	131.84	0.87
JLUE-MOG-10	2.97	132.59	0.97	1518.74	18.13	0.96	0.90	168.61	0.86
JLUE-MOG-11	2.56	168.64	0.93	1520.82	74.13	0.99	1.11	237.43	0.98

Table S5. The water quality parameters of distilled water, tap water and river water.

	COD (mg·L^{-1})	**TN (mg·L^{-1})**	**TP (mg·L^{-1})**	**NO_3^--N (mg·L^{-1})**	**NH_4^+-N (mg·L^{-1})**	**SS (mg·L^{-1})**
Distilled Water	n.d.	0.50	0.04	n.d.	n.d.	n.d.
Tap Water	n.d.	6.45	0.01	n.d.	0.05	n.d.
River Water	24.00	16.24	0.13	5.83	0.10	1.00

[a)] n.d. means not detected

Table S6. Cost estimation for the production of typical JLUE-MOG-10 per unit weight.

Cost	Materials	Used amount/ Duration	Unit Price (RMB)	Total Price (RMB)
Raw materials	$Fe(NO_3)_3·9H_2O$	0.1050 g	0.02 per gram	0.0021
	$Tb(NO_3)_3·6H_2O$	0.1179 g	0.010 per gram	0.0012
	TATB	0.1576 g	0.07 per gram	0.011
	Ethanol	1 mL	5.0 per liter	0.005
	DMSO	5 mL	11.5 per liter	0.058
Net amount			0.25 per gram	

Table S7. FCCD experimental design and related CTC removal efficiencies by JLUE-MOG-10.

Run	Initial pH	Initial CTC Concentration ($mg \cdot L^{-1}$)	JLUE-MOG Dosage ($g \cdot L^{-1}$)	CTC Removal Efficiency (%)
1	2.0	125	1.00	44.50
2	10.0	50	0.50	72.17
3	2.0	50	1.50	66.04
4	6.0	125	1.00	91.01
5	6.0	125	1.50	93.63
6	10.0	200	1.50	93.12
7	6.0	50	1.00	97.20
8	6.0	125	1.00	92.02
9	10.0	125	1.00	76.27
10	6.0	125	1.00	92.02
11	10.0	50	1.50	92.97
12	6.0	200	1.00	91.85
13	6.0	125	1.00	94.68
14	2.0	50	0.50	56.00
15	6.0	125	1.00	90.84
16	2.0	200	0.50	41.65
17	6.0	125	1.00	92.82
18	2.0	200	1.50	47.54
19	10.0	200	0.50	75.24
20	6.0	125	0.50	81.83

Table S8. ANOVA for the optimized FCCD model.

Source	Sum of Squares	df	Mean Square	F Value	P-value Prob > F	
Model	6456.55	9	717.39	126.85	< 0.0001	significant
A-Initial pH	2372.84	1	2372.84	419.58	< 0.0001	
B-Initial CTC Concentration	122.39	1	122.39	21.64	0.0009	
C-JLUE-MOG Dosage	440.82	1	440.82	77.95	< 0.0001	
AB	162.64	1	162.64	28.76	0.0003	
AC	64.68	1	64.68	11.44	0.0070	
BC	6.27	1	6.27	1.11	0.3172	
A^2	2193.71	1	2193.71	387.91	< 0.0001	
B^2	95.70	1	95.70	16.92	0.0021	
C^2	2.20	1	2.20	0.39	0.5464	
Residual	56.55	10	5.66			
Lack of Fit	46.67	5	9.33	4.72	0.0568	not significant
Pure Error	9.88	5	1.98			
Cor Total	6513.11	19				
Std. Dev.	2.38		R^2		0.9913	
Mean	79.17		$R_{Adj}{}^2$		0.9835	
C.V. %	3.00		$R_{Pred}{}^2$		0.9656	
PRESS	224.28		Adeq Precision		35.06	

Table S9. FCCD design validation at optimized conditions.

Number	pH	CTC Concentration ($mg \cdot L^{-1}$)	JLUE-MOG Dosage ($g \cdot L^{-1}$)	Removal efficiency (Predicted) (%)	Removal efficiency (Actual) (%)
1	6.0	50	1.00	100	96.96
2	7.1	61	1.02	100	96.60
3	7.1	51	0.89	99	93.90

Table S10. Comparison of CTC detection limit by various sensors.

Sensor	Analyte	Detection limit	References
Metal–organic coordination polymer(Zn(bix))	CTC	19 nM	64
CdTe QDs@ZIF-8 composite	CTC	37 nM	65
TSA/BSA-Au/AgNCs probe	CTC	64 nM	66
IL1-SMIP/MWCNT-IL/GCE	CTC	80 nM	67
JLUE-MOG-7	CTC	520 nM	33
FHBA@ZIF-8@Eu-GMP	TC	60 nM	68
[Cd(L)(chdc)·(H_2O)]n	TC	76 nM	69
carbon dots	TC	170 nM	70
JLUE-MOG-9	CTC	79 nM	**This work**

Table S11. The recoveries of CTC in distilled water by the measurements of JLUE-MOG-9 based on a smartphone.

Spiked Concentration ($mg \cdot L^{-1}$)	Found ($mg \cdot L^{-1}$)	Recovery (%)	RSD (%)
15	14.12	94.11	1.22
25	30.78	123.13	2.44
35	35.78	102.24	1.23

Table S12. The recoveries of CTC in distilled water, tap water and river water by the measurements of JLUE-MOG-9@paper based on a smartphone.

Spiked	Distilled Water			Tap Water			River Water		
concentration ($mg \cdot L^{-1}$)	Found ($mg \cdot L^{-1}$)	Recovery (%)	RSD (%)	Found ($mg \cdot L^{-1}$)	Recovery (%)	RSD (%)	Found ($mg \cdot L^{-1}$)	Recovery (%)	RSD (%)
15	16.13	107.52	5.88	15.49	103.26	3.72	13.67	91.11	4.89
25	27.43	109.71	8.42	27.16	108.65	10.22	26.96	107.85	10.94
35	38.24	109.26	6.39	35.84	102.39	4.49	36.27	103.62	7.51